



Photoemission from Free Particles and Droplets

Journal Article

Author(s):

[Ban, Loren](#) ; [Yoder, Bruce L.](#); [Signorell, Ruth](#) 

Publication date:

2020-04

Permanent link:

<https://doi.org/10.3929/ethz-b-000412513>

Rights / license:

[In Copyright - Non-Commercial Use Permitted](#)

Originally published in:

Annual Review of Physical Chemistry 71(1), <https://doi.org/10.1146/annurev-physchem-071719-022655>

Funding acknowledgement:

786636 - Droplet Photoelectron Imaging (EC)

125760 - Molecular Ultrafast Science and Technology (MUST) (SNF)

172472 - Phase Transitions of Ultrafine Aerosol Particles: Condensation, Freezing, and Metal Formation in Confined Systems (SNF)

Photoemission from Free Particles and Droplets

Loren Ban, Bruce L. Yoder, Ruth Signorell

ETH Zürich, Laboratory of Physical Chemistry, Vladimir-Prelog-Weg 2, 8093 Zürich

lbان@ethz.ch; yoderb@ethz.ch, rsignorell@ethz.ch

ORCID ID Signorell: 0000-0003-1111-9261

ORCID ID Ban: [0000-0002-9312-2984](https://orcid.org/0000-0002-9312-2984)

Corresponding author: rsignorell@ethz.ch

Keywords: photoelectron spectroscopy, condensed phase, electron scattering, attosecond, optical resonance, surface and interface

Abstract (max. 150 words)

Intriguing properties of photoemission from free, unsupported particles and droplets were predicted nearly 50 years ago, though experiments were a technical challenge. The last decades have seen a surge in the field, due to advances in aerosol technology (generation, characterization, and transfer into vacuum), the development of photoelectron imaging spectrometers, and finally advancement in the fields of vacuum ultraviolet and ultrafast light sources. When performing photoemission studies, particles and droplets offer several advantages. For example, photoemission spectra are dependent on the particle's size, shape and composition providing a wealth of information, which allows for the retrieval of genuine electronic properties of condensed phase. In this review, focused on sub-micron, dielectric particles and droplets, we will explain the utility of photoemission from such systems, summarize several applications from literature, and provide some thoughts on future directions for studies.

1. INTRODUCTION

Nanometer and sub-micron sized particles and droplets are ubiquitous in the Earth's and planetary atmospheres as well as in interstellar space, where they are involved in diverse chemical and physical processes. Particulate matter is also of broad relevance in various technical processes, and is exploited for the study of fundamental processes in condensed matter. A question that has intrigued scientists for decades is to better understand why and how some of their properties differ from those of bulk materials; i.e. how do surface, size, shape and confinement alter bulk properties (1; 2). The present review focusses on the photoemission from small, unsupported dielectric particles and droplets (used here to emphasize liquid phase particles) and on the influence of finite-size effects. The term photoemission refers to the emission of photoelectrons from materials induced by ionizing electromagnetic radiation.

What is unique to the photoemission of small dielectric particles and droplets? A major factor arises from the interaction of the ionizing radiation with these particles, which leads to characteristic spatial variations of the intensity of the ionizing radiation inside the particles. This effect is exemplified in Figs. 1a and c for the two limiting cases referred to as “nanofocusing” and “shadowing”, respectively (3-10). **Nanofocusing** is a resonance phenomenon, which occurs for particles that absorb only weakly at the wavelength of the ionizing radiation; i.e. the imaginary part k of the complex index of refraction $N = n + ik$ is small at this wavelength (n is the real part of the refractive index). The particle acts as an optical resonator, which enhances the average light intensity inside the particle compared with the incident light intensity (4; 7-12) typically by factors up to 10-20. The enhancement is however not uniform throughout the particle. In the case shown in Fig.1a, most of the intensity is localized in an intense hot spot (hence the name nanofocusing) close to the particle's surface on the far side of the incident light. What is the effect on photoelectron images? Photoelectrons are preferentially formed in regions of high light intensity inside the particle with a probability determined by the local light intensity. In the case of nanofocusing, photoelectrons are therefore preferentially emitted from the intensity hot spot and detected in the right half plane of the experimental velocity map photoelectron images shown in Fig. 1b. Furthermore, the overall light enhancement increases the total photoelectron yield in particles compared with bulk samples. **Shadowing** (Fig.1c) dominates when the particle absorbs the ionizing radiation strongly; i.e. when k is high at the corresponding wavelength. In this case, the local intensity is highest at the side of the particle that faces the incoming light. Electrons are thus preferentially emitted from that side and most of the electrons are recorded in the left half plane of the velocity map image (Fig.1d) (3-7). By changing the particle size and/or wavelength of the light the conditions can be tuned between the two limiting cases nanofocusing and shadowing (7; 13). This results in uniquely comprehensive information inscribed in particle photoemission data which can be exploited, for example, to learn about electron scattering in the condensed phase (section 4).

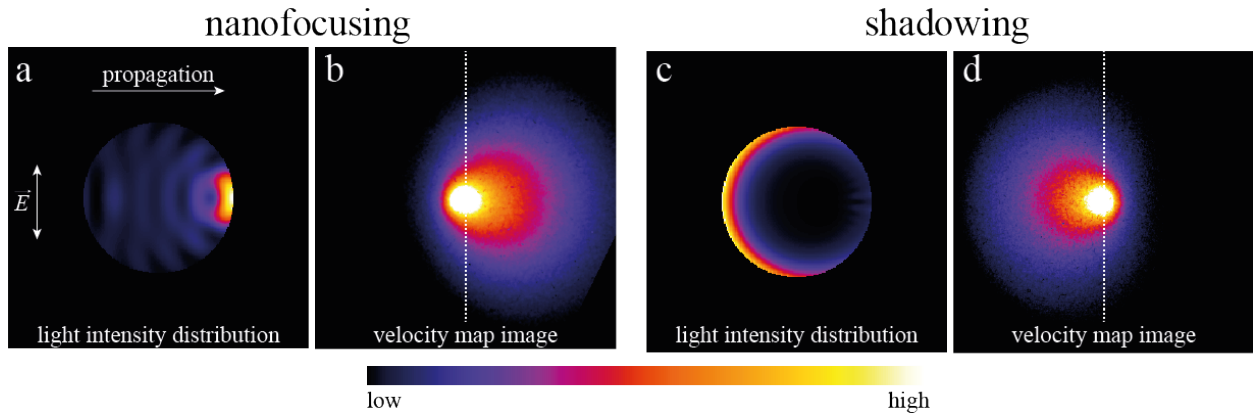


Figure 1: Nanofocusing and shadowing. Nanofocusing (a,b) for 266 nm incident light and shadowing (c,d) for 93 nm incident light in dioctyl phthalate droplets (7). Panels (a) and (c) show the calculated light intensity in a plane through the center of the droplet (250 nm in diameter) spanned by the directions of polarization (\vec{E}) and propagation of the incident light. Panels (b) and (d) show corresponding experimental photoelectron images. The dashed white line divides the left and right half planes of the photoelectron image. Figure adapted from Reference (7) with permission; copyright 2016 Elsevier.

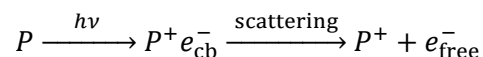
Nanofocusing and shadowing are usually of interest in submicron to micron-sized dielectric particles. Smaller systems (dipole scatterers (4)), such as for example dielectric clusters, are generally too small to exhibit these optical confinement effects. For this reason, this article does not review contributions on photoemission and photodetachment of large clusters (see e.g. (14-16)); and because of their very specific properties it does also not include photoemission studies in superfluid helium droplets (e.g. (17; 18)). Nanofocusing and shadowing do not occur inside metallic particles (4), so that these systems are also not reviewed here. Since we focus on free dielectric particles and droplets in beams (“aerosol particles”), we do not include investigations on photoemission electron microscopy of particles, which generally exclude droplets and can suffer from the influence of the supporter.

Among the pioneering work is the contribution from Watson, who was probably the first to investigate photoelectron emission from dust grains in the context of heating of interstellar clouds by enhanced photoemission (3; 19) The following years saw photoemission from small particles addresses in various contexts. Arnold and Hessel, for example, suggested photoemission from single levitated particles to determine ionization energies (20). Burtscher, Siegmann, Schmidt-Ott and coworkers exploited enhanced photoemission from small particles for aerosol analysis (21; 22), while Niesser and coworkers used laser-induced photoemission to probe polycyclic aromatic hydrocarbon coatings on aerosol particles (23; 24). In relation to these photoemission studies, Hall and Beeman employed electron beams to investigate secondary electron emission (25). Ziemann and McMurry further improved and used these secondary

electron yield measurements to probe organic films on aerosol particles (26). For the early works, experimental studies on particle photoemission were hampered by experimental challenges. With the improvement of particle generation methods and air-vacuum transfer device, the development of new light sources, and the invention of new photoelectron imaging techniques (section 2), particle photoemission is experiencing a revival (6-10; 27-40). This article reviews the recent progress and the current state of the field, and addresses remaining challenges and future opportunities.

2. PHOTOELECTRON IMAGING OF PARTICLES AND DROPLETS

The photoionization process of a particle/droplet P is represented by



where $h\nu$ is the photon energy of the ionizing radiation. The generated conduction band electron (e_{cb}^-) undergoes elastic and inelastic scattering before escaping to vacuum (e_{free}^-) where its photoelectron kinetic energy (eKE) and photoelectron angular distribution (PAD) are detected (41; 42). Inelastic scattering reduces the measured eKE, so that the genuine electron binding energy, $eBE = h\nu - E_{sca}(h\nu) - eKE$, is obtained from the photon energy, the energy-dependent scattering of the electron in the particle, $E_{sca}(h\nu)$, and the recorded electron kinetic energy. Due to the lack of electron scattering data, $E_{sca}(h\nu)$ is often neglected in condensed phase photoelectron spectroscopy (section 4). Electron scattering has a particularly strong influence on the PADs, generally reducing the value of the measured anisotropy compared to that of the genuine.

A sketch of a typical state-of-the-art particle/droplet photoemission imaging spectrometer is shown in Figure 2 (5-8; 10; 28; 30; 34; 37; 38; 40; 43-48). It consists of a particle generation unit, size-selection devices, an air-vacuum transfer device, a light source, and a photoelectron imaging spectrometer.

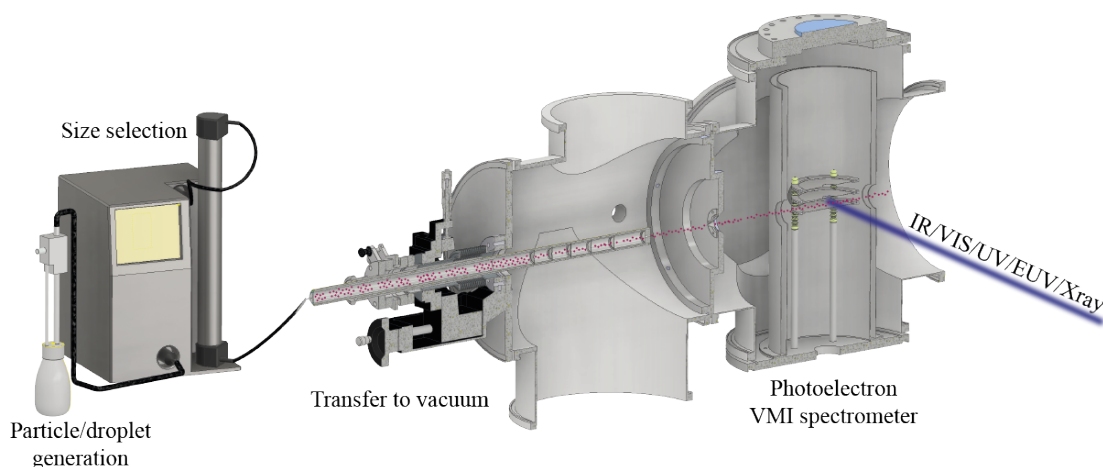


Figure 2: Sketch of a typical experimental setup (13; 43) consisting of a particle generation unit, particle size-selection devices, an interface for the particle transfer into vacuum, light sources to ionize the particles, and a photoelectron spectrometer.

Most of the used particle/droplet technologies are adopted from aerosol science and ref. (49) provides an overview on some of the different generation and sizing methods. Generally, particle generation, size selection and transfer into vacuum is more difficult for submicron-sized particles/droplets than for particles/droplets of many microns in size. These challenges are particularly important for volatile droplets where solutions to accurate sizing and transfer to vacuum are yet to be found. Larger monodisperse particles (typically of several ten microns in size) can be generated by ultrasonic atomization of liquids and solutions, avoiding the need for size selection. However, these advantages come at the expense of low particles number concentration compared with other generation methods. Electrospray is a method for producing monodisperse submicron particles with the caveat that these particles are highly charged and may need subsequent neutralization. High concentrations of small polydisperse particles of less than a few microns in size are generated by pneumatic atomization (nebulization) of liquids and solutions. Solid particles can be produced from solution particles obtained from atomization methods by subsequent drying (diffusion dryers, spray pyrolysis etc.). Particle synthesis from the gas phase - i.e. evaporation and subsequent condensation of material onto particles - has the advantage to generate high purity particles in contrast to atomization techniques which suffer from impurities in the solvent. Polydisperse non-volatile and low-volatility particles/droplets can be size selected before transfer into vacuum, e.g. with electric mobility particles sizers, at the expense of strongly reduced particle number concentrations (28; 49).

The development of the Aerodynamic Lens (ADL) in 1995 by McMurry and coworkers was a milestone for the controlled transfer of particles from ambient pressure into vacuum (50; 51). It yields narrow particles beams in vacuum that are well confined to the centerline of the particle beam. More recently, ADLs were even reported for particles in the low nanometer range, the focusing of which is difficult because of the low inertia and high diffusion (45; 52). Size selection for small volatile droplets was performed with an aerodynamic-mechanical selector (ADMS), which is based on aerodynamic guiding and mechanical selection (7). Other routes that are pursued for submicron to micron sized volatile droplets are vacuum compatible gas dynamic virtual nozzles (GDVN) and simple nozzle injectors which produce monodisperse droplet trains and tightly focused droplet beams, respectively (53; 54).

Many different photon sources with widely varying photon energies and temporal resolutions (from continuous sources to attosecond pulses) are available for particle photoemission experiments. This includes synchrotron radiation sources, free electron lasers and a variety of table-top light sources. Particularly attractive are the new ultrafast VUV to soft X-ray femtosecond and attosecond laser light sources based on high harmonic (HH) generation and time-preserving high-harmonic monochromators (55; 56) that are developing into standard laboratory sources. They have opened up the possibility to perform novel pump-probe and streaking experiments (section 5). A current difficulty with the application of some of these new laboratory laser sources can arise from their low average light intensity, which in combination with the low target density of particles/droplets in beams can result in sensitivity issues.

Hemispherical electron analyzers (31; 34), magnetic bottle/electron time-of-flight spectrometers (36; 45), and velocity map imaging (VMI) photoelectron spectrometers (5; 8; 10; 13; 38; 40; 43; 46; 57-59) are used for the measurement of photoelectron yields, photoelectron kinetic energy distributions and photoelectron angular distributions. The introduction of the VMI to probe particle photoemission has been a major step forward as it is currently the most straightforward way to obtain fast detailed information about the photoelectron kinetic energy and angular distribution. Its major advantages are the very high (4π) collection efficiency and the angular multiplexing; i.e. the possibility to record the whole angular range in one images instead of recording narrow angular slices sequentially as in other methods. However, VMI is limited to the measurement of relatively low kinetic energies, and the cylindrical symmetry required for the reconstruction of the VMI images (60-64) is not always present in particle/droplet spectra, e.g. when nanofocusing or shadowing occur. As discussed in ref. (13), the later can constrain the retrieval of accurate eKE spectra. Figure 3a shows as an example a dioctyl phthalate (DOP) droplet photoelectron VMI image recorded after excitation with 266 nm light. The image has a strongly anisotropic intensity distribution. This angular distribution of photoelectrons does not exhibit cylindrical symmetry along the polarization axis, typically required for the reconstruction and extraction of the eKE spectrum in gas-phase experiments. Since most of the available reconstruction programs exploit the cylindrical symmetry of photoemission, careful analysis is required to obtain quantitative eKE spectra. For example, Figure 3b shows the image obtained by

reconstructing the right half of the experimental image along the laser propagation axis. Essentially the same image is obtained by reconstructing along the polarization axis. However, the eKE spectra retrieved from these reconstructions are clearly different (Figure 3c) because they correspond to a center slice of the 3D photoelectron distribution (insets in Figure 3c) that is assumed to be cylindrically symmetric about the reconstruction axis. We have performed simulations comparing reconstructed and ‘true’ eKE distributions (from scattering simulations, section 4) and observed that the spectrum retrieved from reconstruction along the polarization axis can deviate from the ‘true’ spectrum significantly. These deviations can be largely removed if reconstruction is performed along the propagation axis, due to the often existing cylindrical symmetry about this axis. One should keep in mind, that quantitative eKE spectra can be obtained from experimental VMI images only in combination with detailed optical and electron scattering models (section 4) if pronounced anisotropy is present in the VMIs (7; 44).

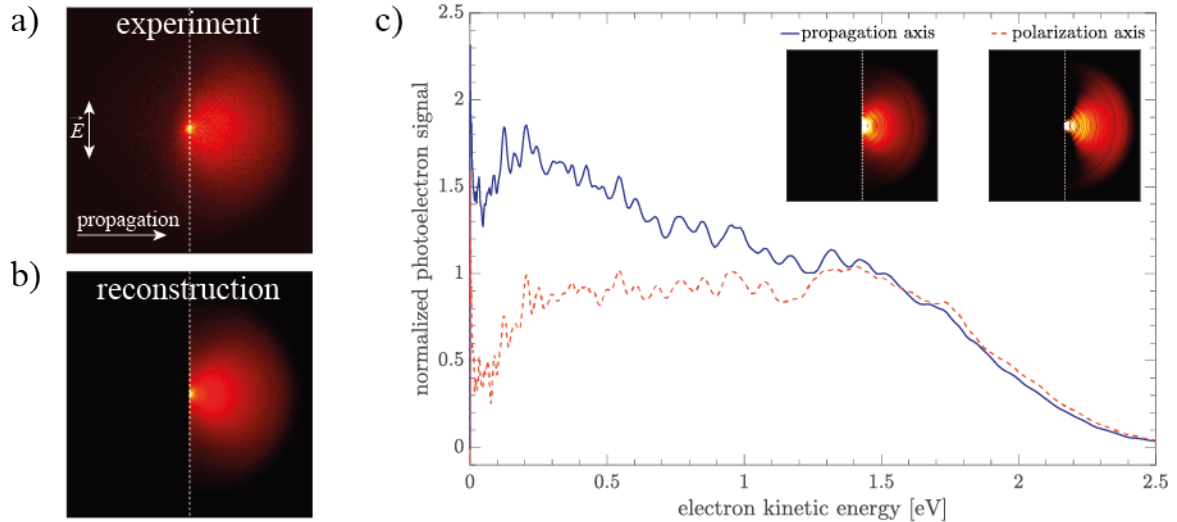


Figure 3: Experimental (a) VMI image for UV-ionized DOP droplets showing strong anisotropy. Image shown in (b) was obtained after reconstructing the right half of the experimental image along the laser propagation direction. The eKE distributions retrieved from reconstructions along the propagation (c, solid blue line) and polarization (c, dashed red line) axes are clearly different. Insets in panel c show center slices of the 3D photoelectron distributions from which the eKE spectrum is extracted.

3. CHARACTERIZATION OF MATTER

Photoemission of particles and droplets for the characterization of condensed matter is an attractive alternative to bulk phase photoemission. Common issues with bulk phase

photoelectron spectroscopy are radiation damage and the buildup of charges. In particle photoemission this is largely avoided due to the constant refreshment of the sample in the particle beam. The particle beam also offers an interaction-free environment, be it with a substrate or with other particles. Another difficulty with volatile bulk phase samples is the incompatibility of high vapor pressures with high vacuum conditions required for photoelectron spectroscopy. This is particularly problematic for angle-resolved photoelectron spectroscopy, which is very sensitive to gas phase scattering. Both the liquid microjet (65) and the particle (7; 31; 34) approach address this issue. An important advantage of the particle technique for angle-resolved studies is the straightforward combination with VMI which provides fast and comprehensive information on the PAD. Particle and droplets also open up the possibility to exploit finite-size effects, such as optical cavity resonances, enhanced photoemission or simply the high surface sensitivity due to their high surface fraction. Last but not least, particle photoemission allows one to access intrinsic particle properties which are relevant to atmospheric and space science as well as technical processes. Even though photoemission of free particles/droplets in beams is a comparatively new direction, the following collection of examples provides an impression of its promises and challenges. Among the later are the rather low target density of particle beams, sample preparation, sizes selection and transfer into vacuum.

3.1 Photoelectron Spectra and Ionization Energies

Particles provide an alternative way for the determination of key electronic properties of condensed matter from photoelectron spectra, such as ionization energies (5-7; 20; 27; 28; 34; 35; 37; 45; 66). Compared with bulk or thin film samples, particles that are constantly refreshed are much less prone to the buildup of charges or radiation damage, which can falsify the measurement of ionization energies. An interesting early approach to determine ionization energies by Arnold and Hessel (20) employed photoemission from single electrostatically levitated microparticles. The ionization energy was derived from the measured change in trapping position caused by photoemission. Later studies were performed on free particle beams in vacuum allowing constant sample renewal (5-7; 27; 28; 35; 45). A notable application to biological materials was presented by Wilson, Leone, Ahmed and coworkers (27). Photoelectron spectra and ionization energies of biological nanoparticles are of interest in astrobiology and for new biological-based detectors and electronics. Their investigation on glycine and phenylalanine-glycine-glycine particles suggests that the polarization energy (the difference in ionization energy of the gaseous and the solid phase) is substantial and plays a role in the ionization process. The interaction of far-ultraviolet photons with Titan aerosols was recently reported in an exciting study by Carrasco, Garcia, Nahon and coworkers (37), which had the aim to provide missing data for photoemission thresholds and ionization cross sections. The low ionization threshold of ~ 6 eV and the very large cross sections they observed reveals that far-ultraviolet photoionization of aerosols is an important process and represents a non-negligible source of electrons in Titan's atmosphere. Where available (e.g. for KI, NaCl, SiO₂) particle photoemission data have so far proven to compare well with corresponding bulk or thin film

data, thus providing an alternative way for the determination of electronic properties of condensed matter.

3.2 Nanofocusing, Shadowing, Circular Dichroism

Particularly appealing are optical phenomena in small particles, such as nanofocusing and shadowing (e.g. Figures 1 and 3 and refs. (3; 6-8; 10; 11; 13; 19; 27; 35; 36; 44; 67)). A detailed analysis of these optical confinement effects requires recording the PADs, which show characteristic asymmetries as shown in Figure 1 and further explained in section 1. These optically induced asymmetries in the photoemission haven been shown to be dependent on the particle size, shape and composition, as well as on the wavelength of the ionizing radiation (6-8; 12; 13; 19; 35; 36; 44). For submicron-sized dielectric particles and droplets, nanofocusing is typically observed in the UV range at photon energies where the particle does not absorb too strongly (7), while shadowing is characteristic in regions of high UV absorption and in the VUV; i.e. in regions where the light attenuation length is much smaller than the particle size (6; 7; 44). Both effects disappear in the X-ray regime where the light attenuation length is on the order of a few micrometers (35). The possibility to tune the conditions between the two limiting cases nanofocusing and shadowing by tuning the wavelength of the ionizing radiation or the particle size makes these optical phenomena particularly attractive. In the early 70ties, Watson recognized that such small particle effects can result in enhanced photoemission yields, with substantial consequences for heating and ionization in interstellar clouds (3; 19). More recently, exploiting these optical confinement effects in photoemission from particles has been suggested as an alternative way to determine electron scattering properties in condensed matter (7; 10; 13; 36; 44) (section 4) and as a probe for plasma formation processes in submicron particles (8) (section 5). Another light induced effect that results in characteristic photoemission anisotropies is observed for chiral particles. Siegmann and coworkers have demonstrated that the interaction of opposite circularly polarized light with chiral particles results in characteristic asymmetries in the photoelectric current (29; 68), an effect that might be exploited in bioaerosol sensors. With the availability of advanced photoemission imaging methods this field of research will likely see more investigations in the coming years.

3.3 Photoelectric Charging

The photoelectric charging mechanisms are in general complex and strongly dependent on the material and the photon energy of the ionizing radiation (21; 28; 30; 69; 70) and references therein). Photoelectric charging studies on free particles allow one to control and vary the charge state – a task that is difficult to achieve for thin films or bulk samples. Studies on UV charging of dielectric particles, for example, have revealed that photoemission yields new information not accessible to the well know diffusion charging (21). It has been proposed and used in field studies as a new possibility to detect small particles where diffusion charging is ineffective, such as combustion aerosols and some natural atmospheric aerosols (21; 69). In this context, we would also like to point to related electron impact charging studies on dielectric particles (71). Detailed information on the charging mechanisms of trapped submicron-sized SiO₂ particles that

are exposed to soft X-ray radiation has been reported by Graf, Grimm, Rühl and coworkers (28; 30; 70). They found a significant change of the number of emitted electrons per absorbed photon as a function of the photon energy, indicating that both primary and secondary electrons contribute to particle charging (30). Furthermore, an increased number of emitted electrons per absorbed photon was found for metal-coated particles (70). Since charges are omnipresent, it is to be expected that many more studies will be devoted to this area of research as free particles and droplets are ideal samples for the investigation of charge effects.

3.4 Surface Composition and Reactions

Surface reactions of particles and droplets are predominantly determined by their surface composition and structure; the knowledge of which is thus highly relevant to atmospheric processes, astrochemistry and technical processes. A range of photoemission investigations has been devoted to the determination of surface composition, including surface coatings (22-24; 31-33; 45; 47; 69; 72-76). The detection of polycyclic aromatic hydrocarbons adsorbed on submicron particles proved particularly successful because it allows the on-line and in-situ determination of the surface coverage and the determination of desorption rates (22-24; 69; 72-74). These studies were performed in the UV range which limits their general applicability to a few specific materials. X-ray photoelectron spectroscopy is element-specific and allows the chemical identification of the constituents in the surface region (31-33; 45; 47; 75). Wilson, Bluhm and coworkers (31) could successfully determine the surface composition of aqueous methanol solutions and found the methanol concentration to be enhanced at the vapor-liquid interface by a factor of about 3 over the bulk value. The complete surface segregation of bromine in mixed NaCl/NaBr particles grown by drying droplets was reported by Miron and coworkers (33). The surface bromine in sea-salt aerosols is a source of atmospheric bromine responsible for ozone depletion. Using a combination of different photoemission techniques, Ahmed, Wilson and coworkers could even quantify heterogeneous reaction of submicron particles (32). They observed an increase in the oxygen to carbon ratio in the ozonolysis of squalene droplets. As the most abundant component on human skin, squalene is a significant ozone reactive compound.

3.5 Aqueous Droplets

As discussed in section 2, the study of high vapor pressure compounds, such as water, by photoemission is challenging because of issues with size selection and transfer into vacuum. It is thus not surprising that aqueous droplets were only recently investigated (7; 31; 34; 35; 66; 77). The ambient pressure photoemission spectrometer by Wilson, Bluhm and coworkers (31) solves this issue by keeping the droplet train at background pressures of several Torr and transferring the electrons into high vacuum by a differentially pumped electrostatic lens system. This setup, however, does not allow to record PADs. Direct transfer of water droplets into high vacuum was recently employed by Wang (34), Signorell (7), Ahmed (35) and coworkers, and combined with VMI (34; 35) to allow for recording the PAD's in addition to kinetic energy spectra. Signorell and coworkers used an ADMS to select only small droplets around 100 nm. Upon transfer into vacuum, such submicron water droplets quickly form supercooled droplets via evaporation,

which prevents them from freezing on the timescale of the experiment because their nucleation times are much longer (7; 34; 78). Recent NEXAFS spectra for broad size distributions with upper sizes close to the micron range provide hints for the coexistence of liquid and ice particles (35). In a recent series of studies (34; 66; 77), Wang and coworkers have investigated the valence electronic structure of biologically or atmospherically relevant organic species in aqueous droplets. Such aqueous droplet studies provide an alternative approach to liquid water microjet studies (65; 79-85). Advantages of the droplet technique are the very high surface fraction, the possibility to access even highly supersaturated solutions and the straightforward combination with VMI. Disadvantages are the low target density and issues with the determination of the concentration after transfer into vacuum.

4. ELECTRON SCATTERING

4.1 Scattering from Photoelectron Imaging

A series of recent publications demonstrate that particle and photoemission experiments offer an alternative way for the determination of electron transport properties in condensed matter (7; 10; 13; 36; 44; 86; 87). This alternative approach appears particularly useful for low-energy electron scattering ($eKE < 20\text{-}50\text{eV}$) in molecular liquids, such as water, which are not easily accessible to thin film or bulk studies because of their high vapor pressure (88; 89). Low-energy electron scattering in molecular system is complicated because of the various interactions of the electron with the intra- and intermolecular vibrations (phonons). The concept of a universal behavior of the energy-dependence of mean free paths and attenuation lengths (“universal curve”) has been disputed over the years (90; 91). For molecular systems, it remains largely unsolved due to the lack of sufficient experimental data. The need of experimental data for low-energy electron scattering in molecular compounds is particularly high because this is a difficult region to access by models which are commonly used to describe high energy scattering (88; 92; 93).

The detailed description of low-energy electron scattering in liquid water is of key importance for the quantitative interpretation of liquid water photoelectron spectra, the modelling of radiation damage processes, radiolysis, and the description of the solvated electron in chemistry and biology (14; 79; 80; 82; 84; 94-103). Detailed scattering parameters; i.e. multiple differential cross sections with respect to electron kinetic energy, energy loss, and scattering angle, only existed for gas phase water (104) and for amorphous ice from energy loss studies of thin films by Sanche and coworkers (99; 105). To substitute the missing liquid data, these ice and rescaled gas phase data were used to describe electron scattering in the liquid state. The error in this approach, however, was unknown. Microjet studies have provided averaged quantities for electron transport in liquid water, such as electron attenuation length (97; 98; 106), but detailed scattering parameters have not yet been reported from microjet experiments. A likely reason for this is the fact that the information content on electron scattering from liquid jets is somewhat limited, because it is not straightforward to analyze and interpret angle-resolved photoemission data.

Compared with microjets, droplet studies allow one to optimize the information content on electron scattering in photoemission data by providing easy access to the PAD through VMI, and by exploiting optical finite-size effects as a function of droplet size and photon energy of the ionizing radiation.

Such photoelectron VMI studies on small water droplets have only recently been performed for electron kinetic energies up to about 6 eV by Signorell and coworkers.(7; 101; 107) The scattering parameters were retrieved from fits of simulated VMI data to experimental VMI data for several different photon energies. The scattering simulations are based on a Monte Carlo solution of the transport equation with the appropriate scattering parameters. As a starting point for the fit, the detailed scattering data given by Michaud, Wen and Sanche for amorphous ice was employed (see refs. (7; 99; 101) for details). This scattering data takes into account the cross sections, energetics, and angular dependences of all relevant scattering processes. Figure 4a shows example experimental (top) and calculated (bottom) VMI photoemission data of water droplets for a photon energy of 15.4 eV. The figure highlights the good agreement between the experiment and the simulation with optimized scattering parameters. The retrieved integral scattering cross sections (integrated over energy loss and deflection angles) for the different scattering channels are shown in Figure 4b. In this very low energy region, inelastic scattering is completely dominated by phonon scattering (blue lines); i.e. by the interaction of the electron with the intra- and intermolecular degrees of freedom. Figure 4b also reveals that the cross sections for liquid water (7; 101) and amorphous ice (99) are within uncertainties (typically less than a factor of two for the liquid data) virtually indistinguishable (see total cross section for liquid water (black line) and for amorphous ice (squares)). This confirms a previous expectation by Sanche and coworkers (99), and resolves a long-standing question regarding the potential difference between amorphous ice and liquid. Preliminary results at higher electron kinetic energies of up to 100 eV (not shown), however, hint at systematic but moderate deviations between liquid and ice at those energies As a side note we would like to add here that recent experiments on large water clusters with a few hundred molecules per cluster revealed that electron scattering cross section in clusters are higher than those of the condensed phase (liquid/ice) but lower than those of the gas phase (108; 109).

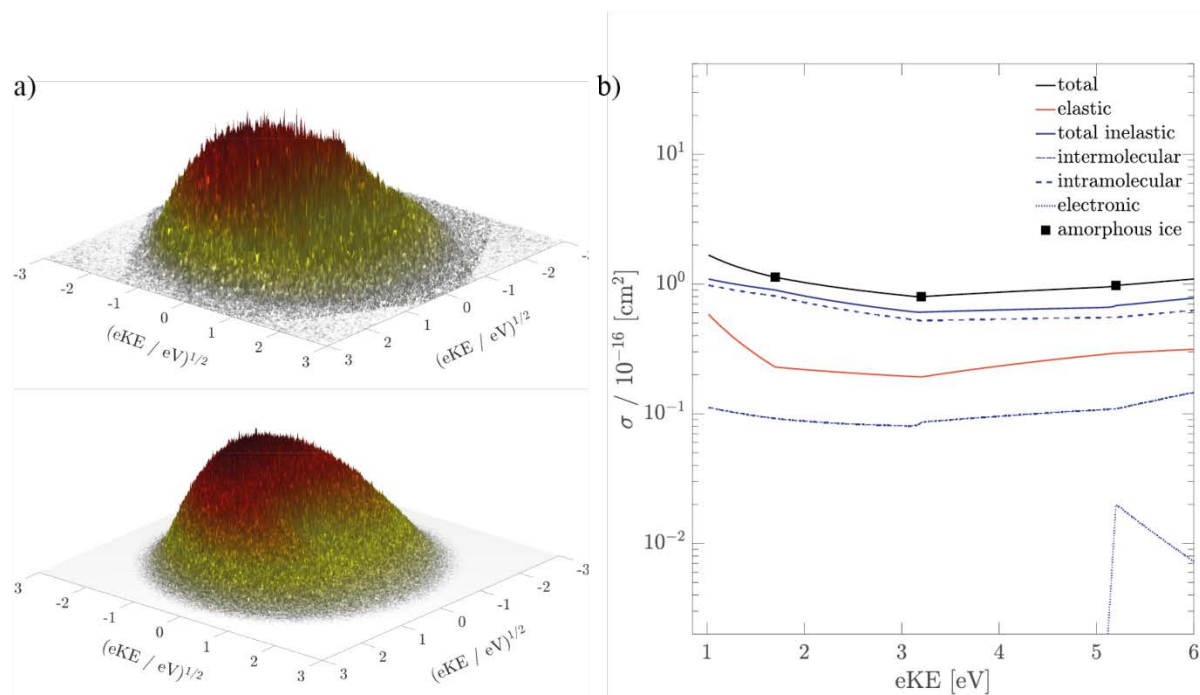


Figure 4: a) Examples of experimental (top) and calculated (bottom) VMI photoemission data of water droplets at a photon energy of 15.4 eV. The histograms show the two-dimensional photoelectron velocity distributions recorded by the electron imaging detector (7; 101) b) Integral electron scattering cross sections of liquid water as a function of the electron kinetic energy (7; 99; 101). The black triangles show the total scattering cross section for amorphous ice from ref. (99). The individual inelastic contributions are represented colour-coded and fall into three groups: Intermolecular vibrational, intramolecular vibrational, and electronic scattering (see refs. (99; 101)).

The viability of the liquid water scattering data has recently been confirmed for angle-resolved photoelectron spectroscopy in the valence region of neat liquid water by the very good agreement that was found between calculated photoelectron anisotropy parameters using the liquid scattering parameters (107) and corresponding experimental data (110). Finally, the availability of the electron scattering data for the liquid state also provides access to the genuine properties of solutes in aqueous solutions, i.e. access to intrinsic properties of the solutes that are not influenced by transport scattering, such as genuine binding energies, genuine photoelectron anisotropies and probing depth. This has recently been demonstrated for photoemission studies of the hydrated electron (101; 102). Not surprisingly, the influence of scattering is extremely pronounced for the PAD, to a degree such that the recorded PADs has lost most of the

information about the genuine PAD. The latter can only be retrieved from the measured data when the influence of electron scattering can be quantified.

4.2 Scattering from Attosecond Streaking

Fennel, Calegari, Kling and coworkers have recently demonstrated for the example of SiO₂ nanoparticles how attosecond streaking experiments of particles can be employed to retrieve information on electron scattering in dielectrics (10; 86). In these streaking experiments, unbound electrons are instantaneously produced by an attosecond EUV pulse, and the momentum change of the electrons induced by a time-delayed near-infrared femtosecond pulse is detected. Essentially, this experiment measures the characteristic damping time of the electron current associated with electronically inelastic collisions. While this approach does not provide information on quasi-elastic scattering (elastic and inelastic phonon scattering) it enables the selective characterization of electronically inelastic mean free paths. It should also be noted that the particle approach for the first time has opened up the possibility to apply attosecond streaking to dielectrics because it prevents accumulation of charges by constantly replenishing the sample.

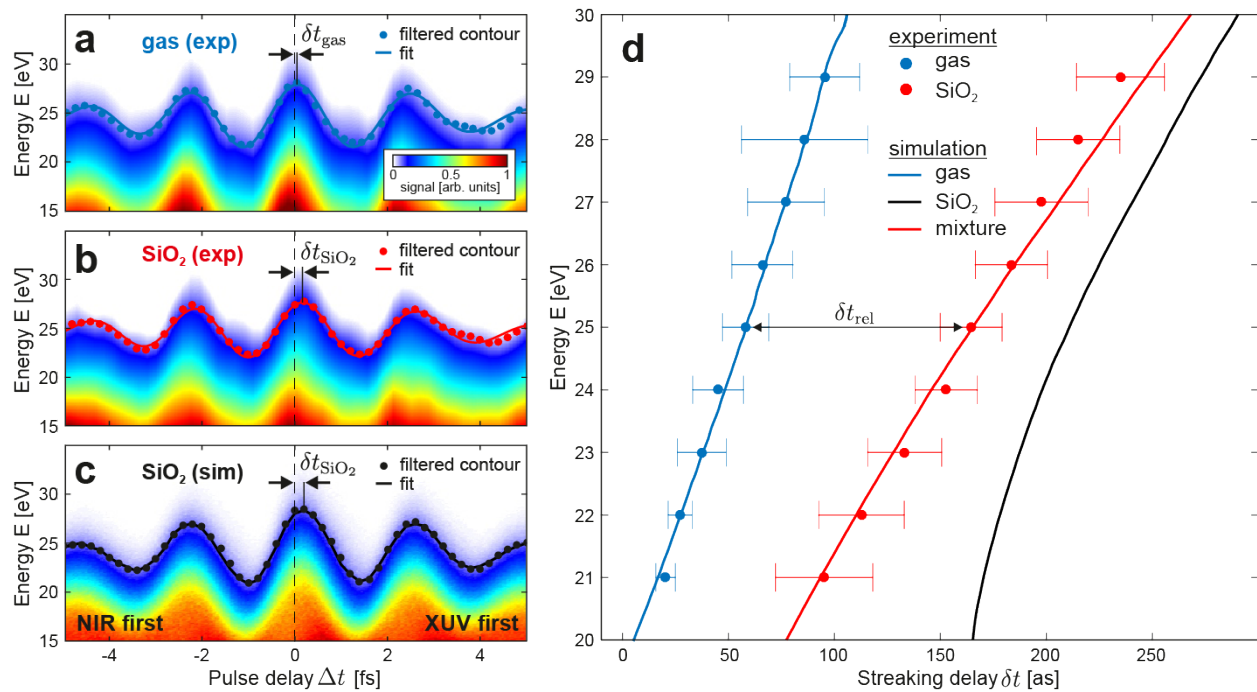


Figure 5: Experimental attosecond spectrograms of the residual gas phase (a) and of SiO₂ nanoparticles (b). Simulated attosecond spectrograms of SiO₂ nanoparticles as predicted by M3C simulations (c). (d) Experimental and simulated energy-dependent streaking delays δt for residual gas (blue), SiO₂ nanoparticles and residual gas (red) and SiO₂ nanoparticles only (black). See ref. (10) for further details. Reprinted by permission from Springer Nature Customer Service Centre GmbH: Published by Springer Nature, Journal Nature Physics, Reference: Seiffert L, *et al.*, Attosecond chronoscopy of electron scattering in dielectric nanoparticles. *Nat. Phys.* 13:766 Copyright (2017).

Figure 5 shows experimental and simulated attosecond spectrograms (a to c) and energy-dependent streaking delays δt (d) for residual gas and SiO₂ nanoparticles. Fennel, Calegari, Kling and coworkers have shown that characteristic energy-dependent inelastic scattering times τ and electronically inelastic mean free paths IMFP can be retrieved from the analysis of δt (see refs. (10; 86) for details). At an eKE of 25eV, a $\tau \sim 370$ as and an IMFP ~ 10 Å was determined for SiO₂ (10). Since attosecond streaking gives access to electron collision timescales in the sub-femtosecond range, it holds promise to provide new insight into the details of electron scattering processes on extremely short timescales which were not accessible so far. Moreover, since the measurement quantities in attosecond streaking and photoelectron imaging (section 4.1) are independent from each other, a direct comparison of the two methods would provide a unique opportunity to compare mean free path data retrieved for the same system but with two complementary experimental approaches.

5. DYNAMICS AND STRONG FIELD EFFECTS

Photoemission investigations that address ultrafast phenomena in free dielectric particles are still comparatively sparse (8; 9; 38; 39; 48; 111-114). One reason might be the low target density of free particles in beams which can cause issues with insufficient sensitivity, for example in pump-probe experiments. Investigations of dynamics can roughly be classified into attosecond and femtosecond studies. Among the attosecond studies are the pioneering streaking experiments on electron scattering in dielectric particles discussed in section 4.2 (10; 86). Another exciting direction are investigations towards the attosecond control of the collective electron motion and directional emission from particles (here SiO₂ particles) using phase-stabilized few-cycle lasers (38; 48; 111-113). They allow unique spatio-temporal control on nanometer spatial and attosecond temporal scales, providing new insight into photoemission processes in the condensed phase. A fundamental understanding of such real-time many-electron dynamics is important for a wide range of potential applications from ultrafast computation to solar energy conversion (see e.g. refs. in (38; 48; 111-113)).

Excitation with few cycle laser fields allows one to restrict the laser interaction with the particle to a few femtoseconds and thus to access the very short time dynamics (38). Even though this is not possible with usual femtosecond laser excitation as typically employed in Coulomb explosion or pump-probe experiments, these studies provide access to a wealth of information on still unexplored dynamics on longer time scales (8; 9; 39; 40; 114). Hickstein et al. have investigated plasma explosion imaging of free NaCl and TiO₂ particles in strong femtosecond infrared laser fields, with the goal to gain insight into unusual light-absorbing properties of particles (8). Their idea was to work under conditions under which the plasma formation threshold is only exceeded at internal light intensity maxima (i.e. for nanofocusing/shadowing

conditions), so that plasma formation only happens in local regions inside the particle. The nanoplasma formation was visualized by recording ion and electron VMIs. Nanofocusing effects could clearly be observed for 100 nm NaCl particles through characteristic asymmetric ion emission, while ion ejection in larger aggregates (50-100 nm) of many small (5 nm) TiO₂ particles was generally found to be symmetric due to the prevention of nanofocusing by the separation of the individual TiO₂ particles.

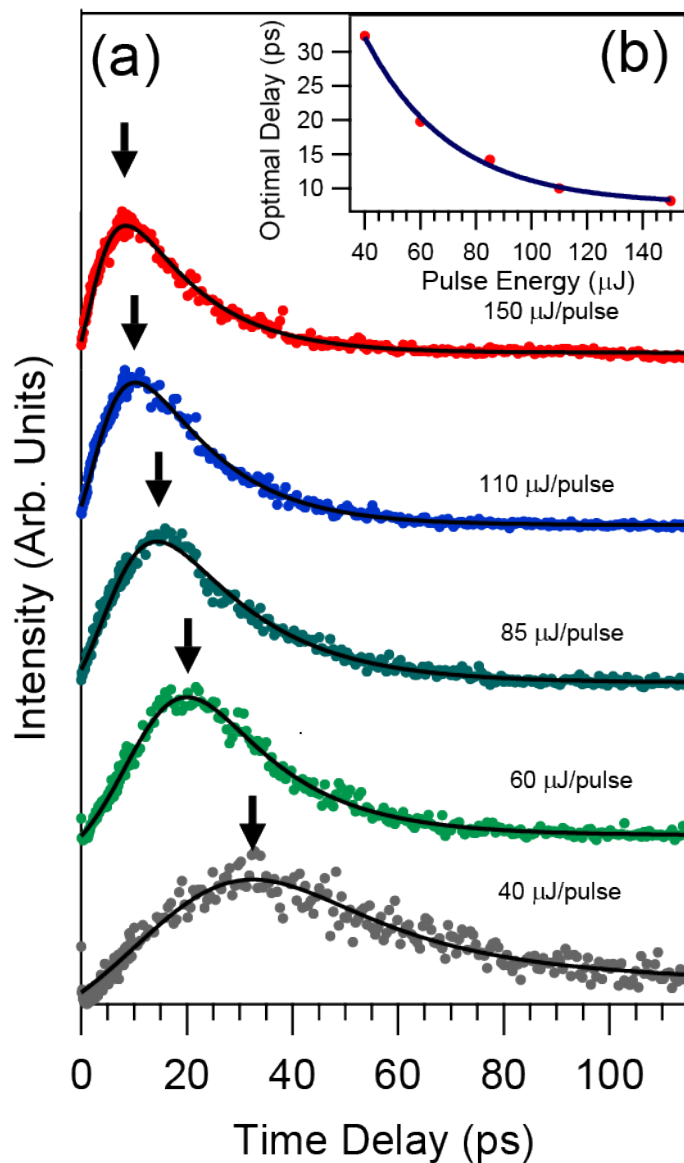


Figure 6: (a) Total electron yields as a function of the time delay between pump pulses of different pulse energies between 150 and 40 μJ and a probe pulse of a constant pulse energy of 60 μJ . (b) Time delays for the maxima in the total electron yields as a function of the different pulse energies (39). Figure reprinted from Reference (39) with permission; copyright 2015 Elsevier.

Fennel, Rühl and coworkers have reported the pump-probe ionization dynamics of free NaCl nanoparticles in intense near-infrared laser pulses by means of total electron yield measurements (39). Fig. 6 shows the total electron yield as a function of the pump-probe delay for different pump pulse energies and a constant probe pulse energy. Compared with single-pulse excitation (not shown in Figure 6, see Fig. 1a in (39)), delay-dependent enhanced electron emission yields are observed for pump-probe excitation, which show maxima at pump-probe delays that depend on the pump pulse energy. Based on model calculations, the enhanced electron emission yield was interpreted in terms of fast pump-induced metallization of the particle and subsequent resonant plasmon heating of the expanding nanoplasma by the probe pulse. The time delay in these studies thus serves as a probe of the transient optical properties of the expanding system. The results from this first investigation were very recently refined in a second study on size-selected particles that provides additional information through angle resolved ion emission experiments (9). Such studies provide direct access to the absorption and photoionization processes in free nanoparticles undergoing resonant heating.

More traditional pump-probe experiments of free dielectric particles and droplets are surprisingly sparse – which is partly a consequence of sensitivity issues. The study by Ellis et al. (40), for example, reports femtosecond pump-probe experiments with the aim to unravel the relaxation dynamics of solvated electrons in oleylamine droplets. Excited state electrons were formed in these droplets by excitation with an EUV pump laser and the subsequent relaxation dynamics of the electron to the ground state of the solvated electron was observed by recording the total photoelectron yield from a time-delayed infrared probe pulse. This study demonstrates the principle feasibility of pump-probe schemes for particle samples, but it also reveals the challenges for future studies to obtain fully energy and angularly resolved photoelectron distributions instead of only total electron yields. Future improvements in the sensitivity of photoemission imaging spectrometers and higher laser repetition rates will be crucial to retrieve time-dependent information on photoelectron energy and angular distributions.

6. SUMMARY POINTS

1. Photoelectron spectroscopy of particles/droplets has experienced a revival in the recent years because of important technical developments in aerosol technology, photoelectron imaging and vacuum ultraviolet and ultrafast light sources.
2. Particle/droplet photoemission provides an alternative – and sometimes a unique - way to access the properties of condensed molecular liquid and solid matter. This includes for example the determination of ionization energies, electronic properties of solutes in aqueous systems, and surface compositions and reactions.
3. Understanding of low-energy electron scattering is crucial for the quantitative interpretation of condensed phase energy- and angle-resolved photoelectron spectra.

Velocity map imaging studies of particles/droplets offer uniquely comprehensive information on electron scattering which can be extracted from photon- and/or size-dependent experiments due to optical confinement effects (nanofocusing and shadowing). Availability of such data is a prerequisite for determining genuine electronic properties of condensed molecular liquid and solid phase systems.

4. Particle/droplet studies have great potential to study electron transport at interfaces as they allow control over the interface size, curvature and composition. The main goal is to gain better knowledge of interface potentials, escape barriers and electron transfer mechanisms (115; 116).
5. Particle/droplet generation methods enable controlled charging, opening the door for studies of charge effects on low-energy electron scattering and electron transfer across interfaces (117). Such studies are not easily performed in bulk, thin film nor liquid jet experiments.
6. The study of electron dynamics in particles/droplets is still in its infancy. Technical developments allowing for higher sensitivity, such as more sensitive photoemission spectrometers and higher laser repetition rates, need to be realized before pump-probe studies on particles/droplets can be routinely performed. Technical improvements should be guided by the idea of generating a small number of electrons from many particles, as opposed to many electrons from only a few particles. For this to happen, effort on increasing the number of particles in the ionization volume will be important.

Acknowledgement

This project has received funding from the European Union's Horizon 2020 research and innovation program from the European Research Council under the Grant Agreement No 786636, and the research was supported by the NCCR MUST, funded by the Swiss National Science Foundation (SNSF), through ETH-FAST, and through SNSF project no. 200020_172472.

Bibliography

1. Signorell R, Reid JP, eds. 2011. *Fundamentals and applications in aerosol spectroscopy*. Boca Raton: Taylor and Francis Books, CRC Press.
2. Sigurbjörnsson ÓF, Firanesco G, Signorell R. 2009. Intrinsic particle properties from vibrational spectra of aerosols. *Annu. Rev. Phys. Chem.* 60:127-46
3. Watson WD. 1972. Heating of interstellar H I clouds by ultraviolet photoelectron emission from grains. *Astrophys. J.* 176:103-10
4. Bohren CF, Huffman DR. 1998. *Absorption and scattering of light by small particles*. New York: Wiley

5. Shu JN, Wilson KR, Ahmed M, Leone SR. 2006. Coupling a versatile aerosol apparatus to a synchrotron: Vacuum ultraviolet light scattering, photoelectron imaging, and fragment free mass spectrometry. *Rev. Sci. Instrum.* 77:043106
6. Wilson KR, Zou SL, Shu JN, Ruhl E, Leone SR, et al. 2007. Size-dependent angular distributions of low-energy photoelectrons emitted from NaCl nanoparticles. *Nano Lett.* 7:2014-9
7. Signorell R, Goldmann M, Yoder BL, Bodi A, Chasovskikh E, et al. 2016. Nanofocusing, shadowing, and electron mean free path in the photoemission from aerosol droplets. *Chem. Phys. Lett.* 658:1-6
8. Hickstein DD, Dollar F, Ellis JL, Schnitzenbaumer KJ, Keister KE, et al. 2014. Mapping nanoscale absorption of femtosecond laser pulses using plasma explosion imaging. *ACS Nano* 8:8810-8
9. Antonsson E, Gerke F, Merkel L, Halfpap I, Langer B, Rühl E. 2019. Size-dependent ion emission asymmetry of free NaCl nanoparticles excited by intense femtosecond laser pulses. *Phys. Chem. Chem. Phys.* 21:12130-8
10. Seiffert L, Liu Q, Zhrebtsov S, Trabattoni A, Rupp P, et al. 2017. Attosecond chronoscopy of electron scattering in dielectric nanoparticles. *Nature Phys.* 13:766
11. Cremer JW, Thaler KM, Haisch C, Signorell R. 2016. Photoacoustics of single laser-trapped nanodroplets for the direct observation of nanofocusing in aerosol photokinetics. *Nat Commun* 7:10941
12. Berg MJ, Wilson KR, Sorensen CM, Chakrabarti A, Ahmed M. 2012. Discrete dipole approximation for low-energy photoelectron emission from NaCl nanoparticles. *J. Quant. Spectrosc. Radiat. Transfer* 113:259-65
13. Amanatidis S, Yoder BL, Signorell R. 2017. Low-energy photoelectron transmission through aerosol overlayers. *J. Chem. Phys.* 146:224204
14. Young RM, Neumark DM. 2012. Dynamics of solvated electrons in clusters. *Chem. Rev.* 112:5553-77
15. Schorb S, Rupp D, Swiggers ML, Coffee RN, Messerschmidt M, et al. 2012. Size-dependent ultrafast ionization dynamics of nanoscale samples in intense femtosecond X-ray free-electron-laser pulses. *Phys. Rev. Lett.* 108:233401
16. Signorell R, Yoder BL, West AHC, Ferreira JJ, Saak C-M. 2014. Angle-resolved valence shell photoelectron spectroscopy of neutral nanosized molecular aggregates. *Chem. Sci.* 5:1283-95
17. Ziemkiewicz MP, Neumark DM, Gessner O. 2015. Ultrafast electronic dynamics in helium nanodroplets. *Int. Rev. Phys. Chem.* 34:239-67
18. Mudrich M, Stienkemeier F. 2014. Photoionisation of pure and doped helium nanodroplets. *Int. Rev. Phys. Chem.* 33:301-39
19. Watson WD. 1973. Photoelectron emission from small spherical particles. *J. Opt. Soc. Am.* 63:164-5
20. Arnold S, Hessel N. 1985. Photoemission from single electrostatically levitated microparticles. *Rev. Sci. Instrum.* 56:2066-9
21. Burtscher H, Scherrer L, Siegmann HC, Schmidt-Ott A, Federer B. 1982. Probing aerosols by photoelectric charging. *J. Appl. Phys.* 53:3787-91
22. Burtscher H, Schmidt-Ott A, Siegmann HC. 1988. Monitoring particulate emissions from combustions by photoemission. *Aerosol Sci. Technol.* 8:125-32

23. Niessner R, Robers W, Wilbring P. 1989. Laboratory experiments on the determination of polycyclic aromatic hydrocarbon coverage of submicrometer particles by laser-induced aerosol photoemission. *Anal. Chem.* 61:320-5
24. Niessner R, Hemmerich B, Wilbring P. 1990. Aerosol photoemission for quantification of polycyclic aromatic hydrocarbons in simple mixtures adsorbed on carbonaceous and sodium chloride aerosols. *Anal. Chem.* 62:2071-4
25. Hall TD, Beeman WW. 1976. Secondary electron emission from beams of polystyrene latex spheres. *J. Appl. Phys.* 47:5222-5
26. Ziemann PJ, McMurry PH. 1998. Secondary electron yield measurements as a means for probing organic films on aerosol particles. *Aerosol Sci. Technol.* 28:77-90
27. Wilson KR, Peterka DS, Jimenez-Cruz M, Leone SR, Ahmed M. 2006. VUV photoelectron imaging of biological nanoparticles: Ionization energy determination of nanophase glycine and phenylalanine-glycine-glycine. *Phys. Chem. Chem. Phys.* 8:1884-90
28. Antonsson E, Bresch H, Lewinski R, Wassermann B, Leisner T, et al. 2013. Free nanoparticles studied by soft X-rays. *Chem. Phys. Lett.* 559:1-11
29. Paul J, Dörzbach A, Siegmann K. 1997. Circular dichroism in the photoionization of nanoparticles from chiral compounds. *Phys. Rev. Lett.* 79:2947-50
30. Grimm M, Langer B, Schlemmer S, Lischke T, Becker U, et al. 2006. Charging mechanisms of trapped element-selectively excited nanoparticles exposed to soft x rays. *Phys. Rev. Lett.* 96:066801
31. Starr DE, Wong EK, Worsnop DR, Wilson KR, Bluhm H. 2008. A combined droplet train and ambient pressure photoemission spectrometer for the investigation of liquid/vapor interfaces. *Phys. Chem. Chem. Phys.* 10:3093-8
32. Jacobs MI, Xu B, Kostko O, Heine N, Ahmed M, Wilson KR. 2016. Probing the heterogeneous ozonolysis of squalene nanoparticles by photoemission. *J. Phys. Chem. A* 120:8645-56
33. Antonsson E, Patanen M, Nicolas C, Neville JJ, Benkoula S, et al. 2015. Complete bromide surface segregation in mixed NaCl / NaBr aerosols grown from droplets. *Phys. Rev. X* 5:011025
34. Su C-C, Yu Y, Chang P-C, Chen Y-W, Chen IY, et al. 2015. VUV photoelectron spectroscopy of cysteine aqueous aerosols: A microscopic view of its nucleophilicity at varying pH conditions. *J. Phys. Chem. Lett.* 6:817-23
35. Kostko O, Xu B, Jacobs MI, Ahmed M. 2017. Soft X-ray spectroscopy of nanoparticles by velocity map imaging. *J. Chem. Phys.* 147:013931
36. Antonsson E, Langer B, Halfpap I, Gottwald J, Rühl E. 2017. Photoelectron angular distribution from free SiO₂ nanoparticles as a probe of elastic electron scattering. *J. Chem. Phys.* 146:244301
37. Tigrine S, Carrasco N, Bozanic DK, Garcia GA, Nahon L. 2018. FUV photoionization of Titan atmospheric aerosols. *Astrophys. J.* 867:164
38. Zharebtsov S, Fennel T, Plenge J, Antonsson E, Znakovskaya I, et al. 2011. Controlled near-field enhanced electron acceleration from dielectric nanospheres with intense few-cycle laser fields. *Nature Phys.* 7:656-62
39. Antonsson E, Peltz C, Plenge J, Langer B, Fennel T, Rühl E. 2015. Signatures of transient resonance heating in photoemission from free NaCl nanoparticles in intense femtosecond laser pulses. *J. Electron. Spectrosc. Relat. Phenom.* 200:216-21

40. Ellis JL, Hickstein DD, Xiong W, Dollar F, Palm BB, et al. 2016. Materials properties and solvated electron dynamics of isolated nanoparticles and nanodroplets probed with ultrafast Extreme ultraviolet beams. *J. Phys. Chem. Lett.* 7:609-15
41. Cooper J, Zare RN. 1968. Angular distribution of photoelectrons. *J. Chem. Phys.* 48:942-3
42. Reid KL. 2003. Photoelectron angular distributions. *Annu. Rev. Phys. Chem.* 54:397-424
43. Yoder BL, West AHC, Schläppi B, Chasovskikh E, Signorell R. 2013. A velocity map imaging photoelectron spectrometer for the study of ultrafine aerosols with a table-top VUV laser and Na-doping for particle sizing applied to dimethyl ether condensation. *J. Chem. Phys.* 138:044202
44. Goldmann M, Miguel-Sánchez J, West AHC, Yoder BL, Signorell R. 2015. Electron mean free path from angle-dependent photoelectron spectroscopy of aerosol particles. *J. Chem. Phys.* 142:224304
45. Meinen J, Khasminskaya S, Eritt M, Leisner T, Antonsson E, et al. 2010. Core level photoionization on free sub-10-nm nanoparticles using synchrotron radiation. *Rev. Sci. Instrum.* 81:085107
46. Gaie-Levrel F, Garcia GA, Schwell M, Nahon L. 2011. VUV state-selected photoionization of thermally-desorbed biomolecules by coupling an aerosol source to an imaging photoelectron/photoion coincidence spectrometer: case of the amino acids tryptophan and phenylalanine. *Phys. Chem. Chem. Phys.* 13:7024-36
47. Sublemontier O, Nicolas C, Aureau D, Patanen M, Kintz H, et al. 2014. X-ray photoelectron spectroscopy of isolated nanoparticles. *J. Phys. Chem. Lett.* 5:3399-403
48. Seiffert L, Süßmann F, Zherebtsov S, Rupp P, Peltz C, et al. 2016. Competition of single and double rescattering in the strong-field photoemission from dielectric nanospheres. *Appl. Phys. B* 122:101
49. Biskos G, Vons V, Yurteri CU, Schmidt-Ott A. 2008. Generation and sizing of particles for aerosol-based nanotechnology. *KONA Powder and Particle Journal* 26:13-35
50. Liu P, Ziemann PJ, Kittelson DB, McMurry PH. 1995. Generating particle beams of controlled dimensions and divergence: I. Theory of particle motion in aerodynamic lenses and nozzle expansions. *Aerosol Sci. Technol.* 22:293-313
51. Liu P, Ziemann PJ, Kittelson DB, McMurry PH. 1995. Generating particle beams of controlled dimensions and divergence: II. Experimental evaluation of particle motion in aerodynamic lenses and nozzle expansions. *Aerosol Sci. Technol.* 22:314-24
52. Wang X, Kruis FE, McMurry PH. 2005. Aerodynamic focusing of nanoparticles: I. Guidelines for designing aerodynamic lenses for nanoparticles. *Aerosol Sci. Technol.* 39:611-23
53. DePonte DP, Weierstall U, Schmidt K, Warner J, Starodub D, et al. 2008. Gas dynamic virtual nozzle for generation of microscopic droplet streams. *J. Phys. D: Appl. Phys.* 41:195505
54. Kirian RA, Awel S, Eckerskorn N, Fleckenstein H, Wiedorn M, et al. 2015. Simple convergent-nozzle aerosol injector for single-particle diffractive imaging with X-ray free-electron lasers. *Structur. Dynam.* 2:041717
55. Poletto L, Villoresi P. 2006. Time-delay compensated monochromator in the off-plane mount for extreme-ultraviolet ultrashort pulses. *Appl. Opt.* 45:8577-85

56. Poletto L, Villoresi P, Frassetto F, Calegari F, Ferrari F, et al. 2009. Time-delay compensated monochromator for the spectral selection of extreme-ultraviolet high-order laser harmonics. *Rev. Sci. Instrum.* 80:123109
57. Eppink ATJB, Parker DH. 1997. Velocity map imaging of ions and electrons using electrostatic lenses: Application in photoelectron and photofragment ion imaging of molecular oxygen. *Rev. Sci. Instrum.* 68:3477-84
58. Heck AJR, Chandler DW. 1995. Imaging techniques for the study of chemical reaction dynamics. *Annu. Rev. Phys. Chem.* 46:335-72
59. Whitaker BJ. 2003. *Imaging in molecular dynamics technology and applications (a user's guide)*. Cambridge: Cambridge University Press
60. Dribinski V, Ossadtchi A, Mandelshtam VA, Reisler H. 2002. Reconstruction of Abel-transformable images: The Gaussian basis-set expansion Abel transform method. *Rev. Sci. Instrum.* 73:2634-42
61. Garcia GA, Nahon L, Powis I. 2004. Two-dimensional charged particle image inversion using a polar basis function expansion. *Rev. Sci. Instrum.* 75:4989-96
62. Dick B. 2014. Inverting ion images without Abel inversion: maximum entropy reconstruction of velocity maps. *Phys. Chem. Chem. Phys.* 16:570-80
63. Gerber T, Liu Y, Knopp G, Hemberger P, Bodi A, et al. 2013. Charged particle velocity map image reconstruction with one-dimensional projections of spherical functions. *Rev. Sci. Instrum.* 84:033101
64. Harrison GR, Vaughan JC, Hidle B, Laurent GM. 2018. DAVIS: A direct algorithm for velocity-map imaging system. *J. Chem. Phys.* 148:194101
65. Winter B, Faubel M. 2006. Photoemission from liquid aqueous solutions. *Chem. Rev.* 106:1176-211
66. Chang P-C, Yu Y, Wu Z-H, Lin P-C, Chen W-R, et al. 2016. Molecular basis of the antioxidant capability of glutathione unraveled via aerosol VUV photoelectron spectroscopy. *J. Phys. Chem. B* 120:10181-91
67. Weingartner JC, Draine BT. 2001. Forces on dust grains exposed to anisotropic interstellar radiation fields. *Astrophys. J.* 553:581-94
68. Paul J, Siegmann K. 1999. Large natural circular dichroism in photoionization. *Chem. Phys. Lett.* 304:23-7
69. Zhiqiang Q, Siegmann K, Keller A, Matter U, Scherrer L, Siegmann HC. 2000. Nanoparticle air pollution in major cities and its origin. *Atmos. Environ.* 34:443-51
70. Graf C, Langer B, Grimm M, Lewinski R, Grom M, Rühl E. 2008. Investigation of trapped metallo-dielectric core-shell colloidal particles using soft X-rays. *J. Electron. Spectrosc. Relat. Phenom.* 166-167:74-80
71. Ziemann PJ, Liu P, Kittelson DB, McMurry PH. 1995. Electron impact charging properties of size-selected, submicrometer organic particles. *J. Chem. Phys.* 99:5126-38
72. Steiner D, Burtscher HK. 1994. Desorption of perylene from combustion, NaCl, and carbon particles. *Environ. Sci. Technol.* 28:1254-9
73. Hueglin C, Paul J, Scherrer L, Siegmann K. 1997. Direct observation of desorption kinetics with perylene at ultrafine aerosol particle surfaces. *J. Phys. Chem. B* 101:9335-41
74. Kasper M, Keller A, Paul J, Siegmann K, Siegmann HC. 1999. Photoelectron spectroscopy without vacuum: nanoparticles in gas suspension. *J. Electron. Spectrosc. Relat. Phenom.* 98-99:83-93

75. Antonsson E, Raschpichler C, Langer B, Marchenko D, Rühl E. 2018. Surface composition of free mixed NaCl/Na₂SO₄ nanoscale aerosols probed by X-ray photoelectron spectroscopy. *J. Phys. Chem. A* 122:2695-702
76. Woods E, Konys CA, Rossi SR. 2019. Photoemission of Iodide from aqueous aerosol particle surfaces. *J. Phys. Chem. A* 123:2901-7
77. Lin P-C, Wu Z-H, Chen M-S, Li Y-L, Chen W-R, et al. 2017. Interfacial solvation and surface pH of phenol and dihydroxybenzene aqueous nanoaerosols unveiled by aerosol VUV photoelectron spectroscopy. *J. Phys. Chem. B* 121:1054-67
78. Manka A, Pathak H, Tanimura S, Wölk J, Strey R, Wyslouzil BE. 2012. Freezing water in no-man's land. *Phys. Chem. Chem. Phys.* 14:4505-16
79. Seidel R, Winter B, Bradforth SE. 2016. Valence electronic structure of aqueous solutions: Insights from photoelectron spectroscopy. *Annu. Rev. Phys. Chem.* 67:283-305
80. Chen X, Bradforth SE. 2008. The ultrafast dynamics of photodetachment. *Annu. Rev. Phys. Chem.* 59:203-31
81. Suzuki T. 2012. Time-resolved photoelectron spectroscopy of non-adiabatic electronic dynamics in gas and liquid phases. *Int. Rev. Phys. Chem.* 31:265-318
82. Abel B. 2013. Hydrated interfacial ions and electrons. *Annu. Rev. Phys. Chem.* 64:533-52
83. Riley JW, Wang B, Woodhouse JL, Assmann M, Worth GA, Fielding HH. 2018. Unravelling the role of an aqueous environment on the electronic structure and ionization of phenol using photoelectron spectroscopy. *J. Phys. Chem. Lett.* 9:678-82
84. Elkins MH, Williams HL, Shreve AT, Neumark DM. 2013. Relaxation mechanism of the hydrated electron. *Science* 342:1496-9
85. Arrell CA, Ojeda J, Sabbar M, Okell WA, Witting T, et al. 2014. A simple electron time-of-flight spectrometer for ultrafast vacuum ultraviolet photoelectron spectroscopy of liquid solutions. *Rev. Sci. Instrum.* 85:103117
86. Liu Q, Seiffert L, Trabattoni A, Castrovilli MC, Galli M, et al. 2018. Attosecond streaking metrology with isolated nanotargets. *J. Optics* 20:024002
87. Jacobs MI, Kostko O, Ahmed M, Wilson KR. 2017. Low energy electron attenuation lengths in core-shell nanoparticles. *Phys. Chem. Chem. Phys.* 19:13372-8
88. Naaman R, Sanche L. 2007. Low-energy electron transmission through thin-film molecular and biomolecular solids. *Chem. Rev.* 107:1553-79
89. Ferradini C, Jay-Gerin J-P, eds. 1991. *Excess electrons in dielectric media*. Boca Raton: CRC Press.
90. Powell CJ. 1988. The quest for universal curves to describe the surface sensitivity of electron spectroscopies. *J. Electron. Spectrosc. Relat. Phenom.* 47:197-214
91. Seah MP. 2012. An accurate and simple universal curve for the energy-dependent electron inelastic mean free path. *Surf. Interface Anal.* 44:497-503
92. Shinotsuka H, Da B, Tanuma S, Yoshikawa H, Powell CJ, Penn DR. 2017. Calculations of electron inelastic mean free paths. XI. Data for liquid water for energies from 50 eV to 30 keV. *Surf. Interface Anal.* 49:238-52
93. Olivieri G, Parry KM, Powell CJ, Tobias DJ, Brown MA. 2016. Quantitative interpretation of molecular dynamics simulations for X-ray photoelectron spectroscopy of aqueous solutions. *J. Chem. Phys.* 144:154704
94. Sanche L. 2009. Beyond radical thinking. *Nature* 461:358
95. Alizadeh E, Sanche L. 2012. Precursors of solvated electrons in radiobiological physics and chemistry. *Chem. Rev.* 112:5578-602

96. Herbert JM, Coons MP. 2017. The hydrated electron. *Annu. Rev. Phys. Chem.* 68:447-72
97. Suzuki Y-I, Nishizawa K, Kurahashi N, Suzuki T. 2014. Effective attenuation length of an electron in liquid water between 10 and 600 eV. *Phys. Rev. E* 90:010302
98. Thürmer S, Seidel R, Faubel M, Eberhardt W, Hemminger JC, et al. 2013. Photoelectron angular distributions from liquid water: Effects of electron scattering. *Phys. Rev. Lett.* 111:173005
99. Michaud M, Wen A, Sanche L. 2003. Cross sections for low-energy (1-100 eV) electron elastic and inelastic scattering in amorphous ice. *Radiat. Res.* 159:3-22
100. Turi L, Rossky PJ. 2012. Theoretical studies of spectroscopy and dynamics of hydrated electrons. *Chem. Rev.* 112:5641-74
101. Luckhaus D, Yamamoto Y-i, Suzuki T, Signorell R. 2017. Genuine binding energy of the hydrated electron. *Sci. Adv.* 3:e1603224
102. Yamamoto Y, Karashima S, Adachi S, Suzuki T. 2016. Wavelength dependence of UV photoemission from solvated electrons in bulk water, methanol, and ethanol. *J. Phys. Chem. A* 120:1153-9
103. Stähler J, Deinert J-C, Wegkamp D, Hagen S, Wolf M. 2015. Real-time measurement of the vertical binding energy during the birth of a solvated electron. *J. Am. Chem. Soc.* 137:3520-4
104. Itikawa Y, Mason N. 2005. Cross sections for electron collisions with water molecules. *J. Phys. Chem. Ref. Data* 34:1-22
105. Michaud M, Sanche L. 1987. Total cross sections for slow-electron (1-20 eV) scattering in solid H₂O. *Phys. Rev. A: At. Mol. Opt. Phys.* 36:4672-83
106. Ottosson N, Faubel M, Bradforth SE, Jungwirth P, Winter B. 2010. Photoelectron spectroscopy of liquid water and aqueous solution: Electron effective attenuation lengths and emission-angle anisotropy. *J. Electron. Spectrosc. Relat. Phenom.* 177:60-70
107. Hartweg S, Yoder BL, Garcia GA, Nahon L, Signorell R. 2017. Size-resolved photoelectron anisotropy of gas phase water clusters and predictions for liquid water. *Phys. Rev. Lett.* 118:103402
108. Gartmann TE, Hartweg S, Ban L, Chasovskikh E, Yoder BL, Signorell R. 2018. Electron scattering in large water clusters from photoelectron imaging with high harmonic radiation. *Phys. Chem. Chem. Phys.* 20:16364-71
109. West AHC, Yoder BL, Signorell R. 2013. Size-dependent velocity map photoelectron imaging of nanosized ammonia aerosol particles. *J. Phys. Chem. A* 117:13326-35
110. Nishitani J, West CW, Suzuki T. 2017. Angle-resolved photoemission spectroscopy of liquid water at 29.5 eV. *Structur. Dynam.* 4:044014
111. Süßmann F, Zhrebtsov S, Plenge J, Johnson NG, Kübel M, et al. 2011. Single-shot velocity-map imaging of attosecond light-field control at kilohertz rate. *Rev. Sci. Instrum.* 82:093109
112. Zhrebtsov S, Süßmann F, Peltz C, Plenge J, Betsch KJ, et al. 2012. Carrier-envelope phase-tagged imaging of the controlled electron acceleration from SiO₂ nanospheres in intense few-cycle laser fields. *New. J. Phys.* 14:075010
113. Süßmann F, Seiffert L, Zhrebtsov S, Mondes V, Stierle J, et al. 2015. Field propagation-induced directionality of carrier-envelope phase-controlled photoemission from nanospheres. *Nature Comm.* 6:7944
114. Hickstein DD, Dollar F, Gaffney JA, Foord ME, Petrov GM, et al. 2014. Observation and control of shock waves in individual nanoplasmas. *Phys. Rev. Lett.* 112:115004

115. Gaiduk AP, Pham TA, Govoni M, Paesani F, Galli G. 2018. Electron affinity of liquid water. *Nature Comm.* 9:247
116. Coe JV, Earhart AD, Cohen MH, Hoffman GJ, Sarkas HW, Bowen KH. 1997. Using cluster studies to approach the electronic structure of bulk water: Reassessing the vacuum level, conduction band edge, and band gap of water. *J. Chem. Phys.* 107:6023-31
117. Ban L, Gartmann TE, Yoder BL, Signorell R. *in preparation*